Technology and Spin-Offs From Doppler Global Velocimetry

James F. Meyers
NASA Langley Research Center
Hampton, Virginia

12th International Symposium on the Unification of Analytical, Computational, and Experimental Solution Methodologies
Worcester, Massachusetts
July 6-8, 1995

Technology and Spin-Offs From Doppler Global Velocimetry

James F. Meyers
NASA Langley Research Center
Hampton, Virginia

Abstract

The development of Doppler Global Velocimetry as a flow diagnostic measurement system necessitated several innovations to solve problems found during wind tunnel testing. These innovations ranged from ratioing a data image with a reference image to remove scattered light variations, dewarping the images to remove optical distortions, and to the use of virtual wind tunnels created with 3-D computer animation technology to test potential optical configurations and present the resulting data. The paper describes Doppler Global Velocimetry and its development through laboratory and wind tunnel investigations, and the various techniques used to solve the problems uncovered during these tests. Several of these solutions are presented as potential spin-offs that can enhance and improve a wide variety of global measurement technologies.

Introduction

The development of modern aircraft has become a complicated and expensive undertaking. Characteristics such as fuel economy, environmental impact, and wake turbulence interference must be optimized to be both competitive in the world marketplace and to satisfy international noise regulations. Classic development strategies used a combination of analytical predictions, wind tunnel testing, and prototype flight testing. This approach is no longer adequate because the analytical predictions are often too simplified to uncover flow subtleties, wind tunnel testing suffers from inaccuracies caused by scaling effects, and flight testing is too expensive.

The advent of modern computer technology has provided a potential solution to this dilemma. Since closed form solutions of analytical predictions can not be obtained without extensive simplifying assumptions, iterative techniques, made possible by these new computers, could permit more accurate predictions. The field of Computational Fluid Dynamics (CFD) can provide descriptions of the interactions between the flow field and the airframe. Verification of these predictions require measurements of the flow and its interaction

with the aircraft, but current flight testing has very limited capabilities to measure the needed parameters. A greater potential for CFD verification exists with wind tunnel testing. Wind tunnel instrumentation such as force balances, accelerometers, pitot probes, hot wires, laser velocimetry, etc. is being used to obtain the necessary comparative measurement databases. The resulting statistical and temporal measurements describe the flow or flow interactions at a single spatial location. The flow field is mapped by moving the probes from point to point to obtain the measurement ensemble. This method assumes flow structures remain stationary while the map is acquired. The resulting databases have provided partial verification of the CFD predictions. Limitations exist because sequential measurements can not provide complete descriptions of spatially dependent flow interactions.

This limitation has created the need for the development of global measurement techniques. Currently several technologies are under development for off-body flow measurements: particle image velocimetry and Doppler global velocimetry (velocity); normal and focused schlieren and holography (density); and laser induced florescence (species). Model surface measurement techniques include: pressure sensitive paint (surface pressure); temperature sensitive paint and infrared thermography (surface temperature); Moiré interferometry (surface profiling and model deformation); and electronic optic holography (surface vibration).

For the past five years, one of these techniques, Doppler Global Velocimetry, has been under development at the NASA Langley Research Center. This technology can provide three-component velocity measurements of a flow as it passes through a selected measurement plane. Although the basic principles are very simple, implementation of a wind tunnel measurement system required additional technologies to be developed. Many of these new developments are also applicable to other global measurement techniques. The following is a description of the development program with emphasis on the spin-offs, and how they could be implemented in other global measurement techniques.

Basic Principles

In the manner of the original laser Doppler velocimeter developed by Yeh and Cummins (1964), Doppler Global Velocimetry (DGV) determines the velocity of micron sized particles embedded in the flow by measuring the Doppler shift frequency of light scattered by the particles as they pass through a laser beam. As depicted in figure 1,

scattered light collected by a detector located along the unit vector $\hat{o}$, from particles passing through a laser beam propagating in $\hat{i}$, is Doppler shifted based on a velocity in the direction $(\hat{o} - \hat{i})$. This relationship is expressed by:

$$\Delta\nu = \frac{\nu_o\,(\hat{o}-\hat{i}) \bullet V}{c} \qquad (1)$$

where $\Delta\nu$ is the Doppler shifted frequency, ν_o is the laser frequency, V is the particle velocity, and c is the speed of light.

Instead of heterodyne detection of the Doppler shift frequency as used by Yeh and Cummins (1964), Komine (1990) used the side of an absorption line in Iodine vapor as an optical frequency discriminator. The original system, Komine *et al* (1991), was based on a single-frequency Argon ion laser operating at a wavelength of 514.5 nm. In later work, Komine *et al* (1994) used a pulsed, single-frequency, frequency-doubled Nd:YAG laser with the Iodine vapor cell to demonstrate that the technology could produce instantaneous measurements of a flow field.

The optical transmission function of an Iodine vapor cell for an optical wavelength of 514.5 nm is shown in figure 2. If the laser output frequency was tuned to a point midway along the edge of the absorption line, figure 2, collected scattered light from a stationary object or cloud of particles would be attenuated by 50 percent as the light passed through the vapor. If the object or particle cloud were moving, the attenuation through the vapor increased (or decreased, depending on the direction of movement) by an amount proportional to the scattered light Doppler shift frequency induced by the object's motion, equation (1). Thus, placing an Iodine vapor cell in front of the detector in figure 1 would cause the level of the detector output to be proportional to the velocity of an object or particle cloud passing through the laser beam. It would also be proportional to the total amount of light scattered. Thus influences from particle number density, particle size distribution, and intensity variations across the laser beam must be removed. Placing a beam splitter ahead of the Iodine vapor cell to direct a portion of the collected scattered light toward a second detector would provide an output voltage proportional to the scattered light intensity. This was used as a reference level to produce a normalized signal whose amplitude was influenced only by the Iodine vapor.

Since this approach is based on collected scattered light levels, detecting individual particles, as needed by other laser velocimetry techniques, is not required. Also, since optical heterodyning is not

used, linear detectors such as Charge Coupled Devices (CCD) can be used to measure the scattered light levels. Thus, the input laser beam can be expanded into a sheet to illuminate a desired measurement plane, and the detectors can be replaced by 512x512 pixel CCD video cameras. This Doppler Global Velocimeter, figures 3 and 4, is then equivalent to 262,144 fringe-type laser velocimeters, since each pixel in the video camera is, in effect, a single detector viewing a small volume of flow within the measurement plane. A three-component DGV system can be constructed by using three optical receiver systems located at different angles from the light sheet yielding three output vectors, $\hat{o}_a$, $\hat{o}_b$, and $\hat{o}_c$, equation (1).

The Development of the DGV Concept

The invention of Doppler Global Velocimetry by Komine (1990) suggested that three-component global velocity measurements, with grid spacings comparable to those used in CFD, were possible with a simple optical system. The potential of this concept, along with its simplicity, made it an excellent candidate for development into a flow diagnostics instrument. In 1990 the NASA Langley Research Center began an accelerated program to develop this technology for wind tunnel and flight applications.

The desire by NASA researchers to accelerate the DGV development process prompted a dual-effort approach (Meyers and Komine (1991)). Komine and his team at the Northrop Research and Technology Center were contracted to determine the feasibility of using a pulsed, frequency-doubled Nd:YAG laser as the DGV laser source by NASA Langley (Komine *et al* (1994)). The Northrop program was to determine the necessary laser characteristics for DGV operation, and the potential of a pulsed system for flight applications. At the same time, an in-house effort would construct an Argon-ion laser based system, duplicating the laboratory configuration constructed by Komine (1990). This undertaking would provide an in-house understanding of the technique, and begin its conversion into a wind tunnel measurement system (Meyers (1992)).

The Northrop effort found no operational difference between an Argon ion laser based system and the frequency-doubled Nd:YAG laser based system. The study did find differences in characteristics. A frequency-doubled Nd:YAG laser based system was found to have the following advantages: instantaneous measurements (10 nsec); capable of measuring velocity standard deviation because the short pulse length maintains full turbulence bandwidth; and potentially capable of making flight measurements since shuttered cameras reduce

background light to negligible levels. This configuration was found to have a few disadvantages: the laser line width is 100 MHz compared to 10 MHz for the Argon ion laser which limits the maximum velocity range within the measurement plane; beam forming optics are needed to flatten the output laser power distribution since a cylindrical lens must be used to form the light sheet; and the typical output pulse rate is only 10 Hz. The Argon ion laser based system has greater versatility since a galvanometer-based scanner can be used to establish the light sheet; greater dynamic range since it has a narrow bandwidth; only requires an etalon to obtain single frequency operation; and has greater availability since it is the laser normally used for fringe-type laser velocimetry. On the minus side, this system needs a dark wind tunnel test section to minimize background light, and has less output power than the frequency-doubled Nd:YAG laser. For the remainder of the paper, no differentiation will be made between the two configurations.

The Receiver Optical System

As mentioned above, the receiving optical system, figure 4, consists of a beamsplitter, an Iodine vapor cell, first surface mirror, and two CCD video cameras, each equipped with a 50 mm focal length, 35 mm single-lens-reflex lens modified to attach to the C-mount on the camera. The use of the beamsplitter as the scattered light collector allows each camera to view the laser light sheet along the same optical axis. Ideally with careful alignment, each pixel output in the signal camera could be normalized by the output from the corresponding pixel in the reference camera to yield the velocity dependent image.

Spin-Off: When Pressure Sensitive Paint is illuminated by blue light, the interaction of oxygen with the paint will cause the paint to fluoresce red light with an intensity proportional to the partial pressure of oxygen. Typically, variations in illumination intensity are removed by normalizing the acquired data image with a reference image obtained before the tunnel is started. However, if the model moves or deforms during testing, the reference image will not match the data image, causing measurement errors. If a DGV receiver was modified by replacing the Iodine vapor cell with a transmission notch filter set to the fluorescence wavelength, and a transmission notch filter set to the illumination wavelength was placed in front of the reference camera, proper normalization could be obtained regardless of the model position.

In practice, it is very difficult, if not impossible, to physically align the signal and reference cameras to subpixel accuracies over the entire

image. Although standard horizontal, vertical, pan, tilt, and focus misalignments can be optically corrected, image distortions caused by optical imperfections in the beam splitter, mirror, Iodine vapor cell, or camera lenses, and imperfections in the CCD or its placement can not. In addition, image distortions from tunnel windows and perspective distortions caused by nonorthogonal viewing angles also affect the image quality. Digital image processing technology was selected to correct the acquired images and provide the needed spatial tolerances.

The first step was to generate a target containing a grid of dots at known spacings, figure 5, and place it in the light sheet plane. An acquired image would then be interrogated to determine the centroid location of each dot. These locations provide the data needed to develop the series of warping equations used to dewarp and correct the data images. In theory this process is straight forward. In practice however, it proved to be impossible using standard commercial image processing software. These codes used linear, second order, or third order polynomial regression techniques to curve fit the dot locations. While this approach is capable of removing perspective and scaling distortions, it is incapable of removing minor optical variances. Also, the routine process of determining the dot pattern centroids proved to be difficult because standard techniques use threshold detection to find the dots. Placing the target in a cross flow plane shadows the dots from test section lighting. Additional lights will increase the target illumination, but their intensity distributions contribute to illumination nonuniformity.

Software necessary to accomplish these tasks was developed for a personal computer using Visual Basic for the graphical user interface and FORTRAN for the computations. The determination of the dot centroid locations began by displaying the acquired image for the user to select the dot to be located in the upper left corner of the grid, e.g., dot **a** in figure 5. Next, the dots in the first row, second column (dot **b**) and the second row, first column (dot **e**) were selected. After these selections, the code began processing by high-pass filtering the acquired image with a Sobel filter. Since the dots have a high frequency content, the filtered image could be converted to an isolating mask by hard clipping at a value corresponding to the edge of the dots. An amplitude inverted version of the original image was logically ANDed with the mask yielding a target with only the pixels within the dots having values greater than zero. The centroid for the dot **a** (the upper left corner of the grid) was determined by searching for the smallest square with a zero valued perimeter that would surround the selected location, and calculating the two-dimensional histogram within the square to find the weighted averaged x and y locations. The centroid for dot **b** was then found in the same manner. These two centroids were

used to linearly predict where dot **c** was located. If a nonzero value was found at that location, the centroid was calculated as before. If not, the dot was assumed to be out of focus and thus excluded by the high-pass filter. Then the program selects the predicted position as the centroid location. The second and third centroids were then used to predict the location of dot **d**. This cycle continued for the desired number of columns. After determining the centroid for the selected dot **e**, this location and the location for dot **b** were used to predict the location of dot **f**. The row was then processed as described above. The centroids for the first two columns were determined in the same manner to obtain the needed starting centroids for the remaining rows.

The selected number of rows and columns were used to develop the maximum grid size for an integer number of pixels or grid spacing between each row/column that would fit in 512x512 pixels. The spacing between the first two centroids, dots **a** and **b**, row was divided into the grid spacing to obtain the first linear transfer function. All spacing values between the first and the remaining centroids were multiplied by the first linear transfer function. This process aligned the first two centroids with the first two columns of the final grid, dots **A** and **B**. The second linear transfer function was calculated from the shifted second and third centroids and used to align the third centroid with the third column, dot **C**. The remaining centroids on the first row and the centroids on the remaining rows were aligned with their respective columns in the same manner. Each centroid was also aligned vertically to the appropriate row using the same procedure.

Using these piecewise bi-linear transfer functions, each pixel location in the dewarped image can be mapped back to its equivalent location in the original image. The amplitude at this location can be determined by a weighted average of the amplitudes of the surrounding four pixels based on their distance from the mapped location. For example, three receiver systems were aligned on the left, right, and above the dot target, and tilted 30 degrees out of the target plane. The acquired images from the reference cameras in components A, B, and C are shown in the top half of figure 6. Applying the piecewise bi-linear transfer functions for each camera to its respective image results in the dewarped images shown in the bottom half of figure 6. These images show that the dewarping procedure removes perspective and optical distortions to provide subpixel overlays of the six camera images.

To determine if this dewarping procedure was sufficient to allow the transformation of components A, B, and C to the standard orthogonal components U, V, and W, a spinning wheel was placed in the target plane and illuminated with a single-frequency Argon ion laser. The acquired images were corrected for variations in camera pixel

sensitivity, the background light and camera dark current levels were removed, and the images dewarped to align the six cameras. Each signal image was normalized by its respective reference image to yield maps of Doppler frequency distribution. The resulting images were then corrected for differences in optical transmission characteristics between the signal and reference optical paths. The corrected component maps were then converted to velocity using the Iodine absorption line transfer function, figure 2. The resulting velocity maps are shown in figure 7. The component values at each pixel location were then transformed to the standard, orthogonal U, V, and W component velocities, figure 7. As shown, the velocity distribution in the U component is small and about 0 m/sec indicating insignificant wobble in the wheel. The V and W components show the expected horizontal and vertical velocity distributions.

Spin-Off: Global measurement techniques such as Pressure Sensitive Paint, Temperature Sensitive Paint, Moiré Interferometry, Electronic Speckle Pattern Interferometry, Electronic Optical Holography, and Digital Particle Image Velocimetry, suffer from the same image distortions as DGV. Although Digital Particle Image Velocimetry is the only technique that can utilize the dewarping procedure directly, the other techniques can benefit if the model surface topology is incorporated. Painting dots at known locations on the model surface would provide the necessary dewarping reference points. However, this method does not provide adequate compensation for the three-dimensional model movement or deformation normally found in wind tunnel testing. An alternative approach would pass a light beam through two orthogonal placed Ronchi rulings to illuminate the model with an orthogonal grid of dots. Viewing the dot pattern with cameras placed at three viewing angles would provide data for three-space triangulation procedures and the dewarping reference points. Acquiring images during wind-off and wind-on conditions would provide model movement and deformation details in addition to the data needed to maintain calibration of the chosen global technique.

Wind Tunnel Testing

The first wind tunnel application of three-component DGV was the investigation of the hot, near sonic flow exiting a high-speed civil transport engine model in the NASA Ames 40-x 80-foot Subsonic Tunnel. Since the optical system had to be designed for a tunnel 4800 km away, CAD/CAM, rendering, and animation software was used to develop a computer model of the test section, engine model, and DGV

optical system. Each test section window location was checked to determine the model viewing angles and focal distances to investigate potential locations for the laser input and the three receiver systems. The final locations were chosen based on obtaining the greatest angular separation to maximize coordinate transformation accuracy while minimizing perspective distortions. The animation software was then used to view the light sheet from the camera's viewpoint for each potential position to determine the image magnification as a function of available lens focal lengths along with assessing the resulting perspective distortions. The results of this process are shown in figure 8. Once the DGV measurements were obtained, the results were placed within the light sheet plane in this virtual wind tunnel. Animations viewing the data from various positions within the tunnel help to provide insight into the fluid mechanics since the data is presented within the test environment.

Spin-Off: The use of computer graphics and animations can help design both experimental and computational fluid dynamic investigations since the characteristics of the wind tunnel, model, and measurement instrumentation can be included. The ability to simulate a camera system and determine the characteristics of the viewed image provides the researcher with guidance in configuring the various global measurement techniques to obtain the desired measurements.

The final optical configuration, shown in figure 8, resulted in receiver focal distances from 15.25 m to 17.5 m for the three components. 35-mm Single Lens Reflex (SLR) camera lenses with 135 mm focal lengths and f–numbers of 2.3 were installed on the RS-170 CCD video cameras. The resulting magnification factor of 10 provided a 1.25 mm spatial resolution of the 200 mm diameter jet flow yielding over 160 measurement points across the jet diameter. The laser light sheet was placed nearly orthogonal to the jet axis, 5 cm downstream of the jet exit. The resolved U-component velocity map is shown in figure 9. The velocity image clearly shows the symmetric velocity deficit behind the aft engine cone. The velocity profile along the jet diameter is also shown to illustrate the details of the flow structure and the velocity and spatial resolution capabilities of the DGV technique.

The next investigation was to determine the influence of a trailing business jet model on the position of a wing tip vortex flow generated by a straight wing placed ahead of the jet, figure 10. The investigation was conducted in the Langley 30-x 60-foot Full Scale Tunnel. The receiver optical systems for components A and B were placed in elliptical pods located on the test section floor. The pods were placed symmetrically on each side of the cross flow plane defined by the laser light sheet. These

systems used 100 mm focal length SLR lenses to obtain a 1.25 mm spatial resolution of the 50 mm diameter vortex flow. The focal distance from the receivers to the intersection of the vortex with the light sheet was 7.5 m. The receiver optical system for component C was placed on the top of the flow inlet cone, 18 m from the measurement plane. This receiver used 135 mm focal length SLR lenses to match the 1.25 mm resolutions of the other components.

The major difficulty of this test was not the long focal length or the small size of the vortical flow, but tunnel vibration misaligning the receiver optical systems. The solution was to cross correlate the dewarped reference and signal images to determine how far the cameras misaligned. The signal image was then moved to overlay the reference image by the correlation distance. These distances were typically less than 3 mm. The three receivers were returned to alignment by cross correlating the reference camera images and moving components B and C to overlay component A.

Additionally, this technique could be used to adjust the acquired data to remove random movements of flow structures. For example, the average of 30 frames (60 fields) of the resolved cross-flow velocity component are shown in figure 11 for straight wing settings of 2- and 10-degrees angle of attack. The figures on the left are normal averages of the velocity at each pixel location based only on the number of valid measurements acquired by that pixel. These figures show the motion of the vortex during the measurement period. The figures on the right are averages obtained following cross correlations of the first measurement image with the remaining images, then moving those images to overlay the first. This average provides a view of the vortex flow structure.

Spin-Off: The cross correlation of global measurement images after dewarping can align multiple camera systems in the various global measurement techniques. It is noted that the dewarping process will *flatten* three dimensional images into a two dimensional plane. If the multiple cameras view the same areas, the flattened images will cross correlate. If, however, they do not, or areas are blocked by three dimensional projections, the effectiveness of the cross correlation decreases.

The latest investigation was the study of the flow entering the tail rotor of a Comanche helicopter model conducted in the Langley 14-x 22-foot Subsonic Tunnel. Various configurations were studied in an attempt to isolate the inflow components. Although this investigation proceeded normally, the data images contained circular patterns with deviations nearly equivalent to free-stream velocity. Usually this pattern is negated by the optical transmission correction. However in this case,

the pattern varied between wind-off and wind-on. Since the pressure in the area surrounding the open test section varied with wind speed, the characteristics of the camera lenses changed, altering the pattern spacing. Since these artifacts could not be removed in the normal manner, a band-reject image at the pattern frequency was used to filter the data images. The effectiveness of this process is illustrated in figure 12. While the use of frequency domain image processing techniques does not qualify as a spin-off, it illustrates how these techniques can improve global measurement quality.

Summary

Doppler Global Velocimetry has been described along with its development through wind tunnel testing. Innovations developed to solve problems uncovered during testing were also described. The effects of these innovations on the flow measurements were illustrated using results from several wind tunnel investigations. A number of these developments were highlighted as spin-offs since they can be applied to and improve other global measurement techniques.

References

Komine, H.: *System for Measuring Velocity Field of Fluid Flow Utilizing a Laser-Doppler Spectral Image Converter*. United States Patent 4,919,536, April 24, 1990.

Komine, H.; Brosnan, S. J.; Litton, A. B.; and Stappaerts, E. A.: *Real-Time, Doppler Global Velocimetry*. AIAA 29th Aerospace Sciences Meeting, Paper 91-0337, Reno, NV, January 7-10, 1991.

Komine, H.; Brosnan, S. J.; Long, W. H.; and Stappaerts, E. A.: *Doppler Global Velocimetry Development of a Flight Research Instrumentation System for Application to Non-Intrusive Measurements of the Flow Field*. NASA CR-191490, January 26, 1994.

Meyers, J. F.; and Komine, H.: *Doppler Global Velocimetry - A New Way to Look at Velocity*. **Laser Anemometry: Advances and Applications**, 1991, eds. A. Dybbs & B. Ghorashi, ASME, 1991.

Meyers, J. F.: *Doppler Global Velocimetry - The Next Generation?* AIAA 17th Aerospace Ground Testing Conference, Paper 92-3897, Nashville, TN, July 6-8, 1992.

Yeh, Y.; and Cummins, H. Z.: *Localized Fluid Flow Measurements with a He-Ne Laser Spectrometer*. Applied Physics Letters, vol. 4, no. 10, pp. 176-178, May 1964.

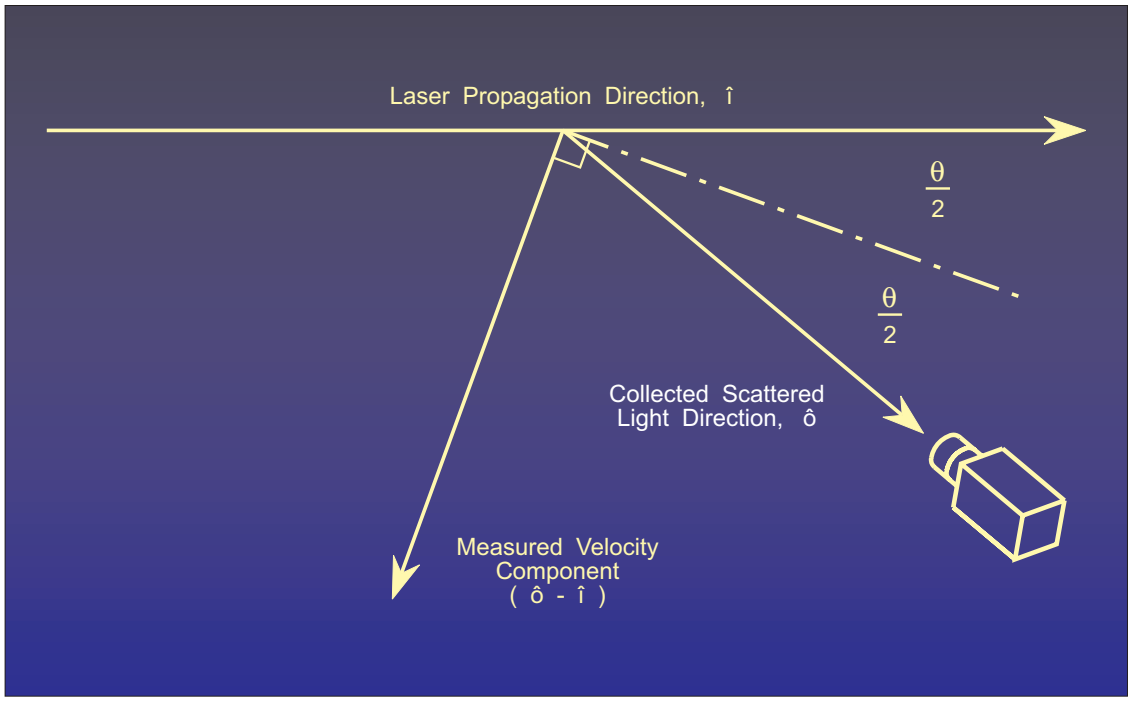

Figure 1. Diagram depicting the velocity measurement direction based on the orientation of the laser propagation direction and the detector location.

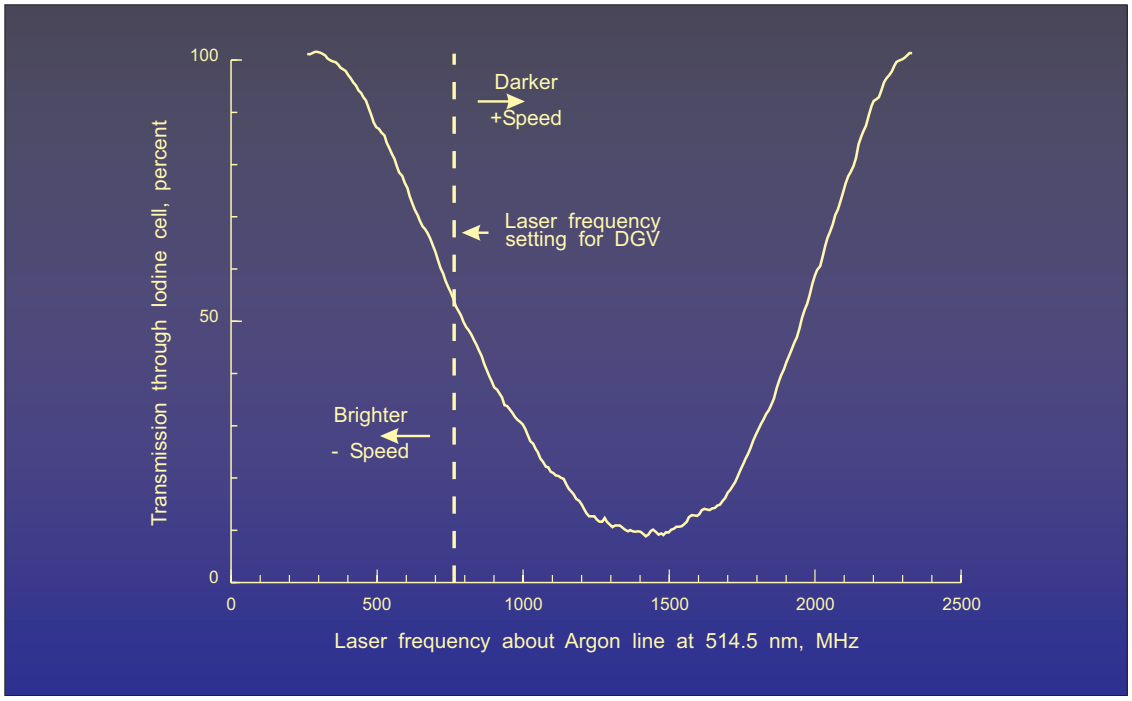

Figure 2. Transfer function of the Iodine vapor cell, IVC.

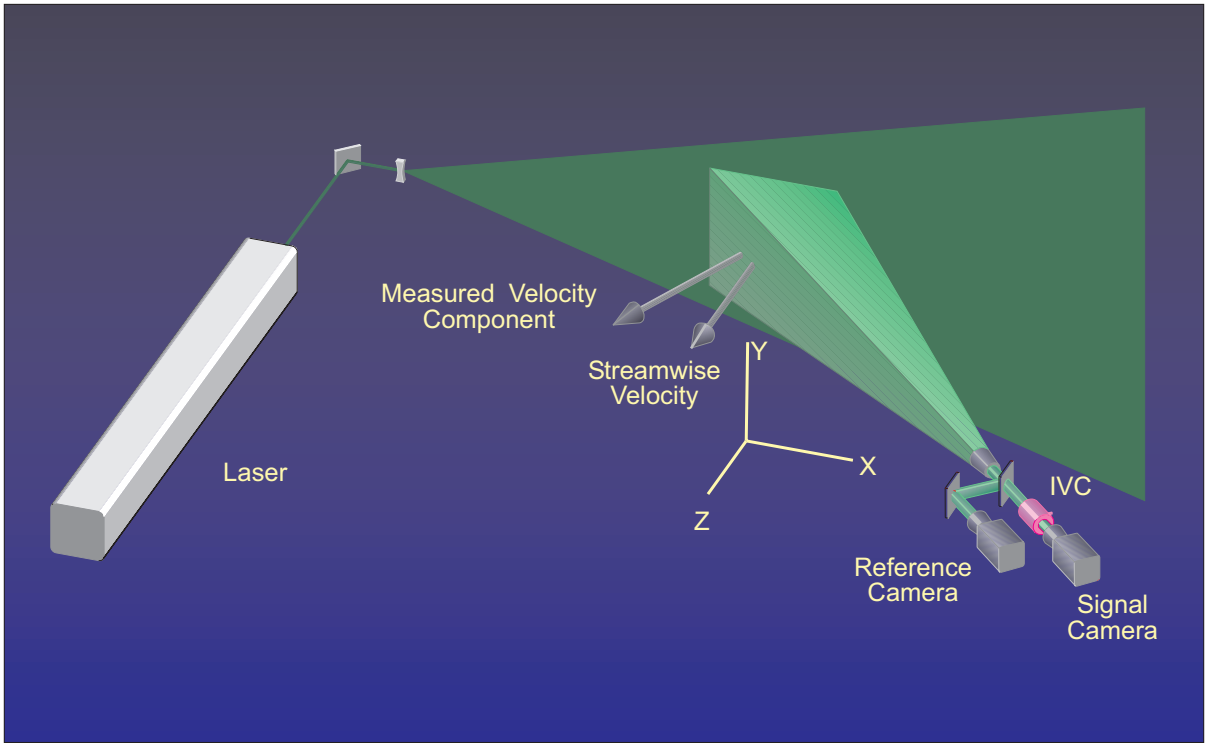

Figure 3. Pictorial view of the Doppler global velocimeter.

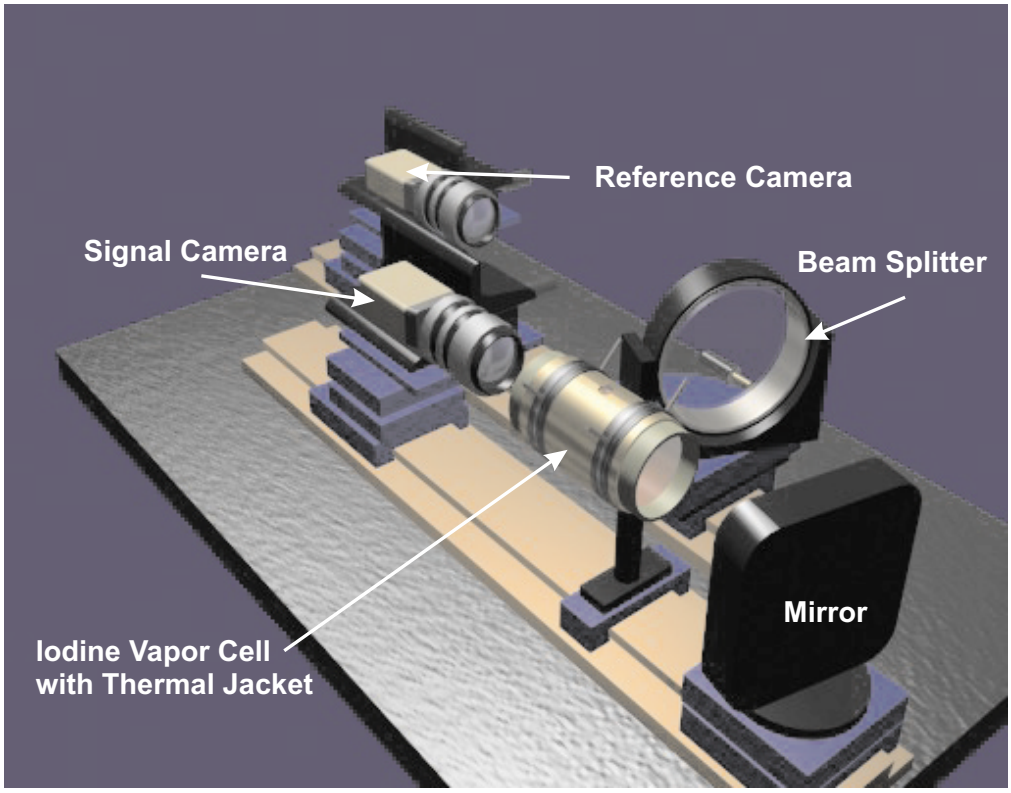

Figure 4. Pictorial view of the receiver optical system.

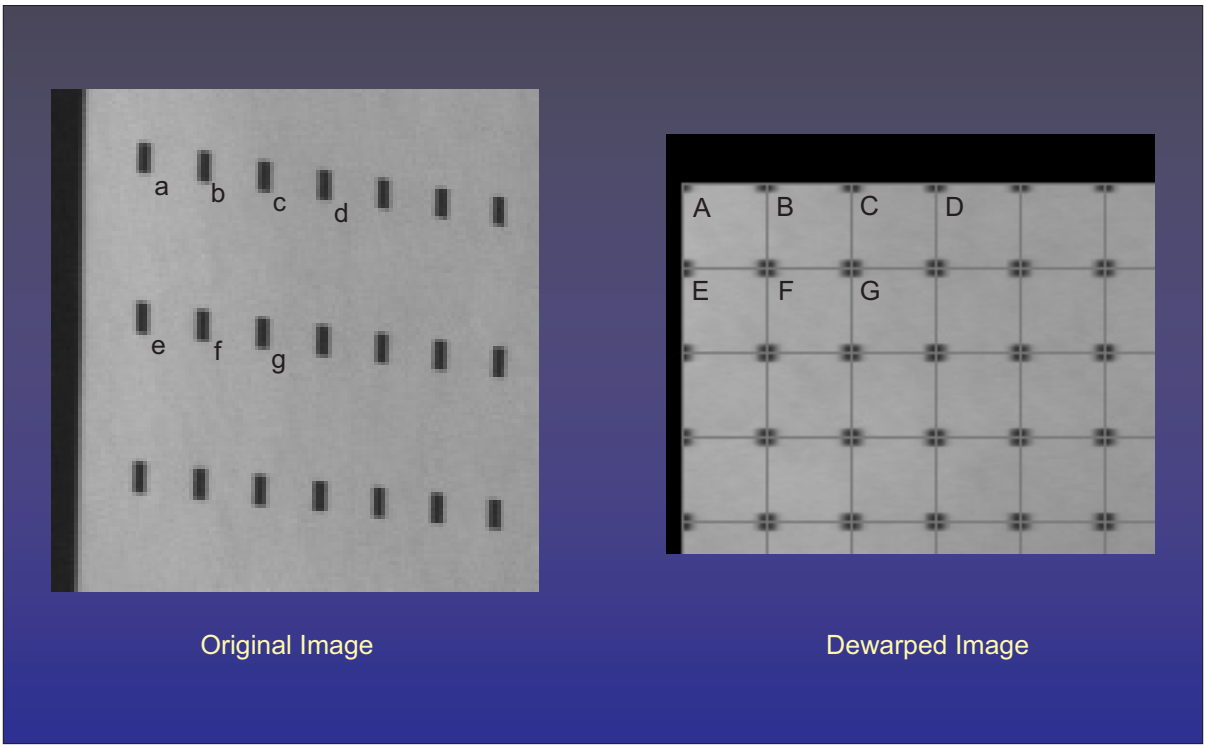

Figure 5. Transposition of the dot locations from the original image to the dewarped version.

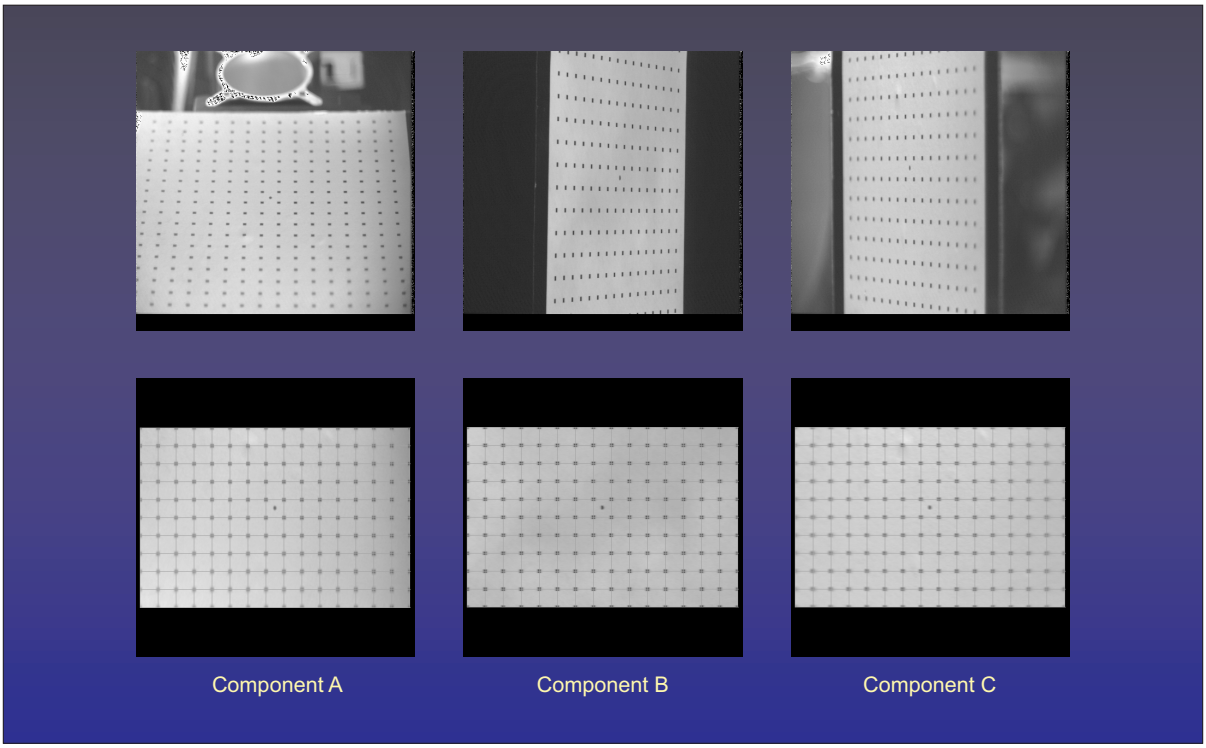

Figure 6. Views of equally spaced dots on a flat card from the left, right, and above with an inclination of 30 degrees from the card plane, before and after warping.

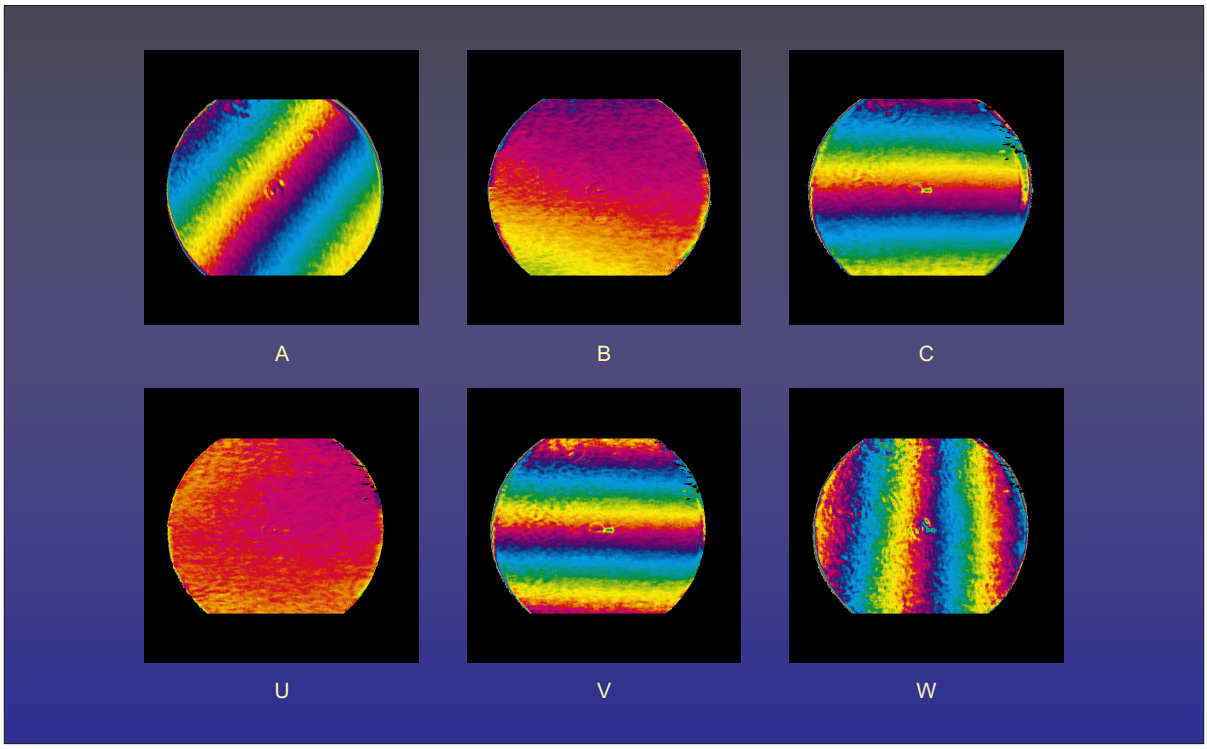

Figure 7. Original and resolved u, v, and w velocity component images of a rotating wheel obtained from the three views shown in figure 6.

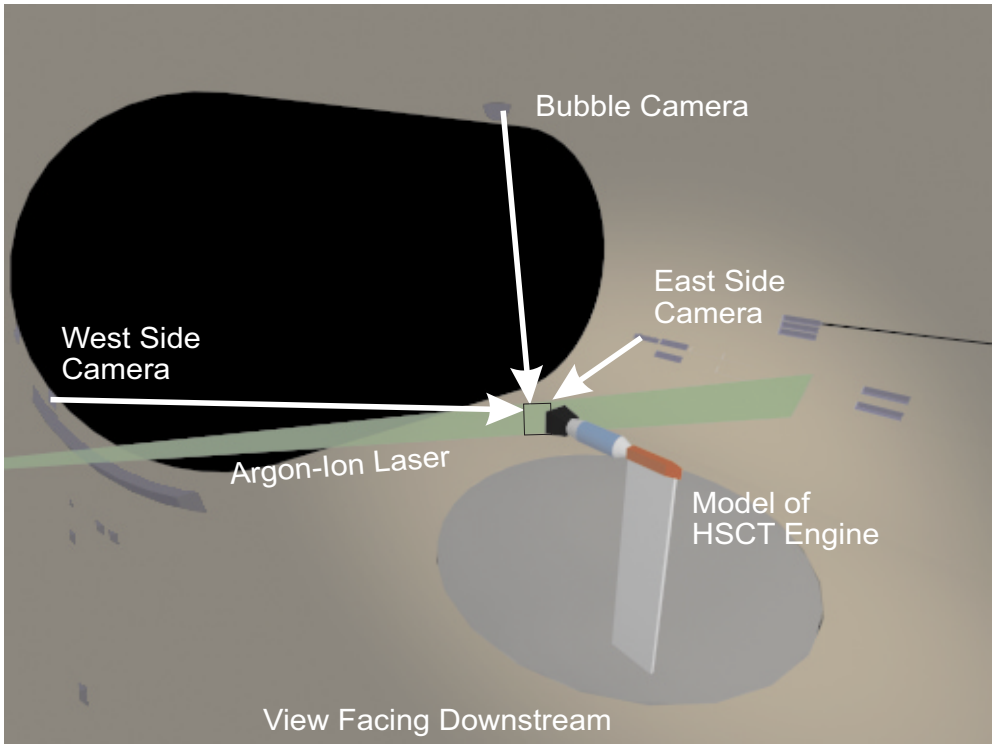

Figure 8. Configuration of the three-component DGV optical system in the NASA Ames Research Center 40-x80-foot Wind Tunnel to measure the flow from a high-speed jet.

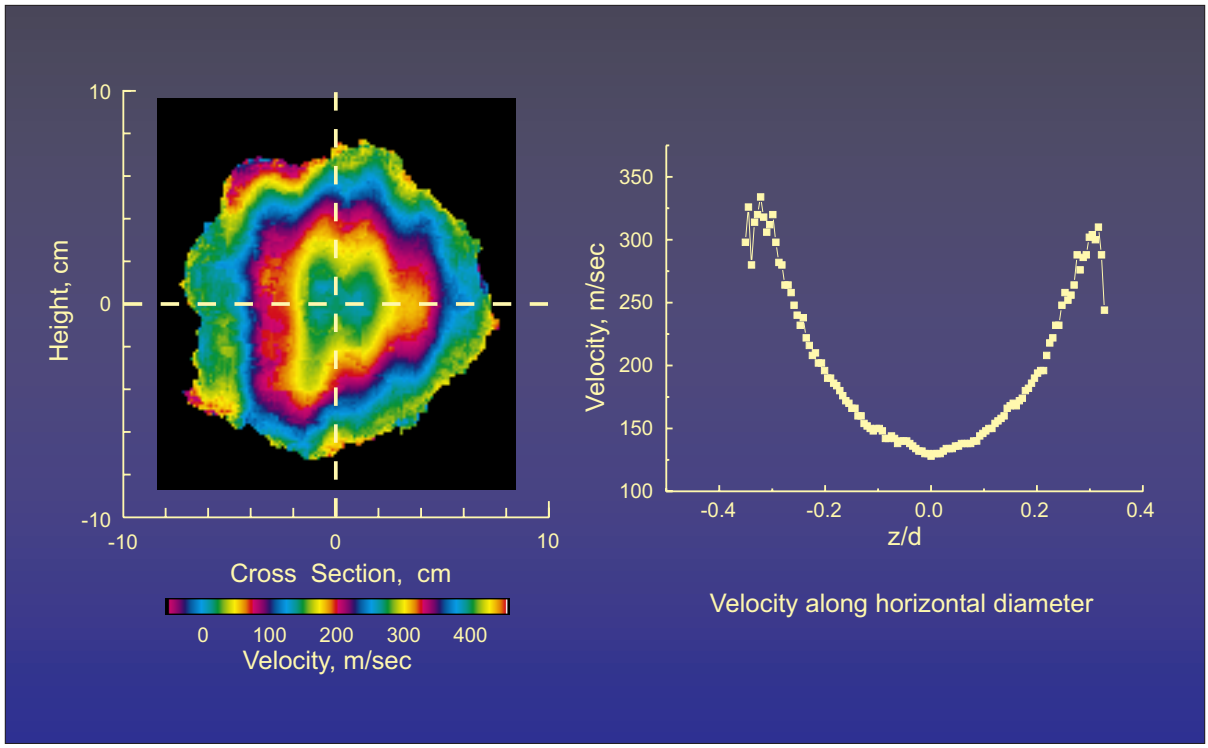

Figure 9. Resolved streamwise component of velocity from the high-speed jet flow operating at 463^{0} C at a free stream Mach number equal to 0.15.

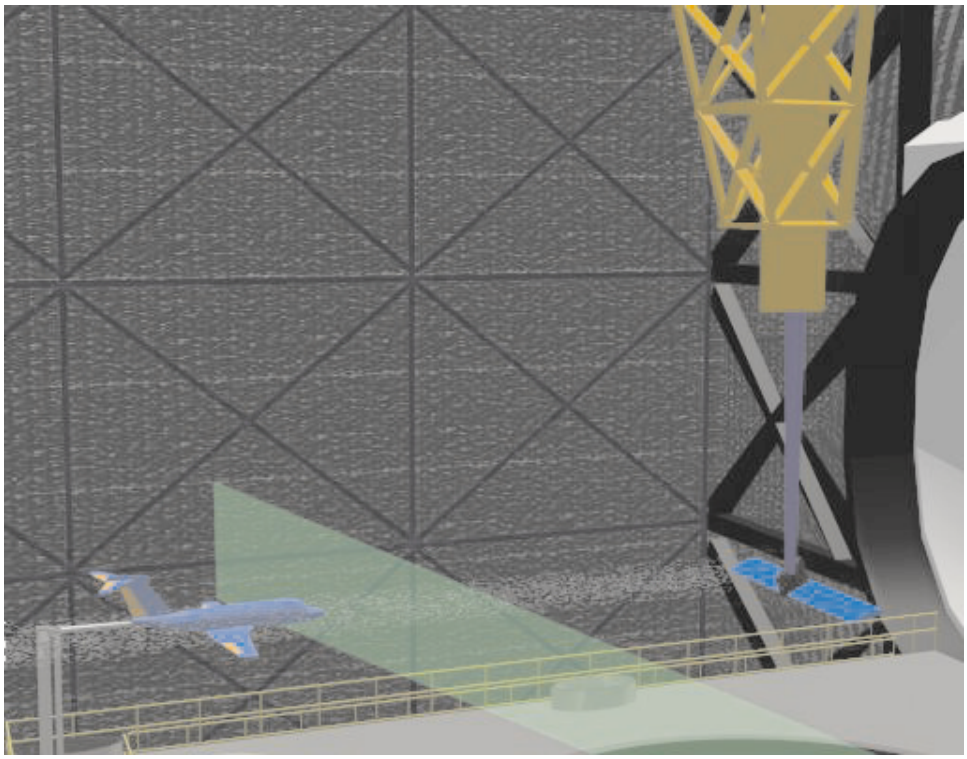

Figure 10. Pictorial view of the wing tip vortex interaction investigation in the Langley 30-x 60-foot Full Scale Tunnel.

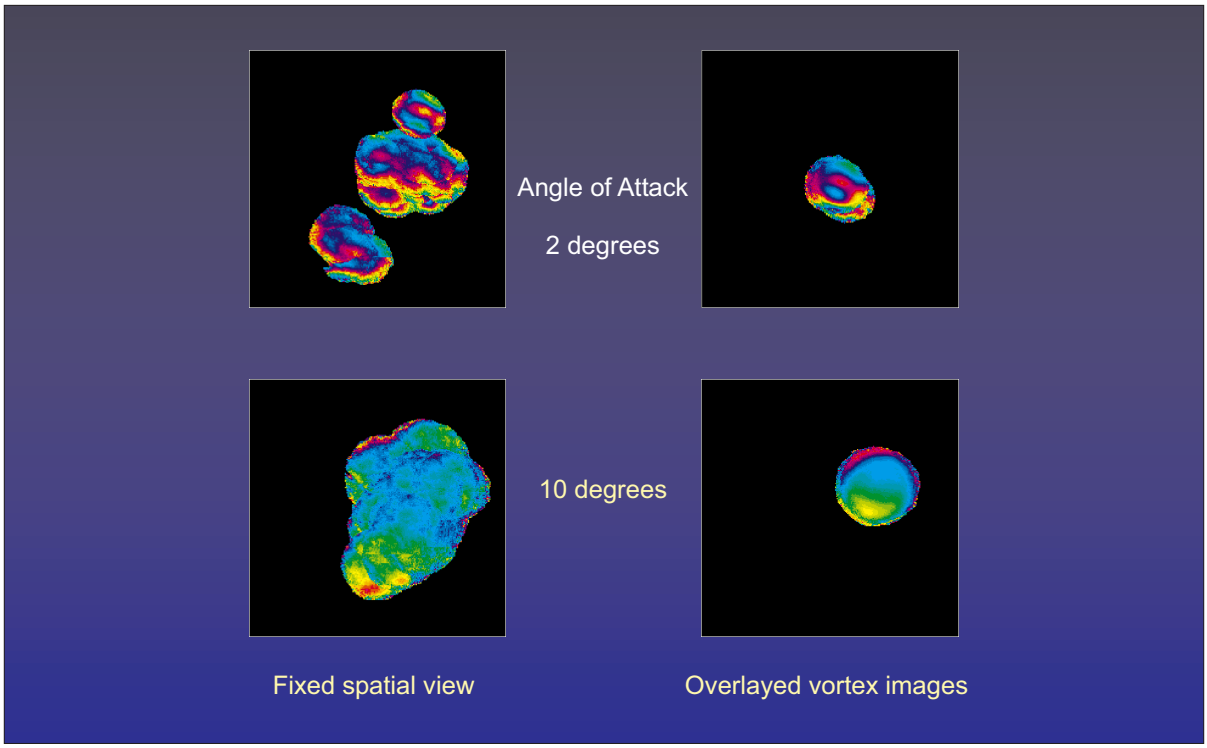

Figure 11. Time averages of the cross flow velocity component of the wing tip vortex.

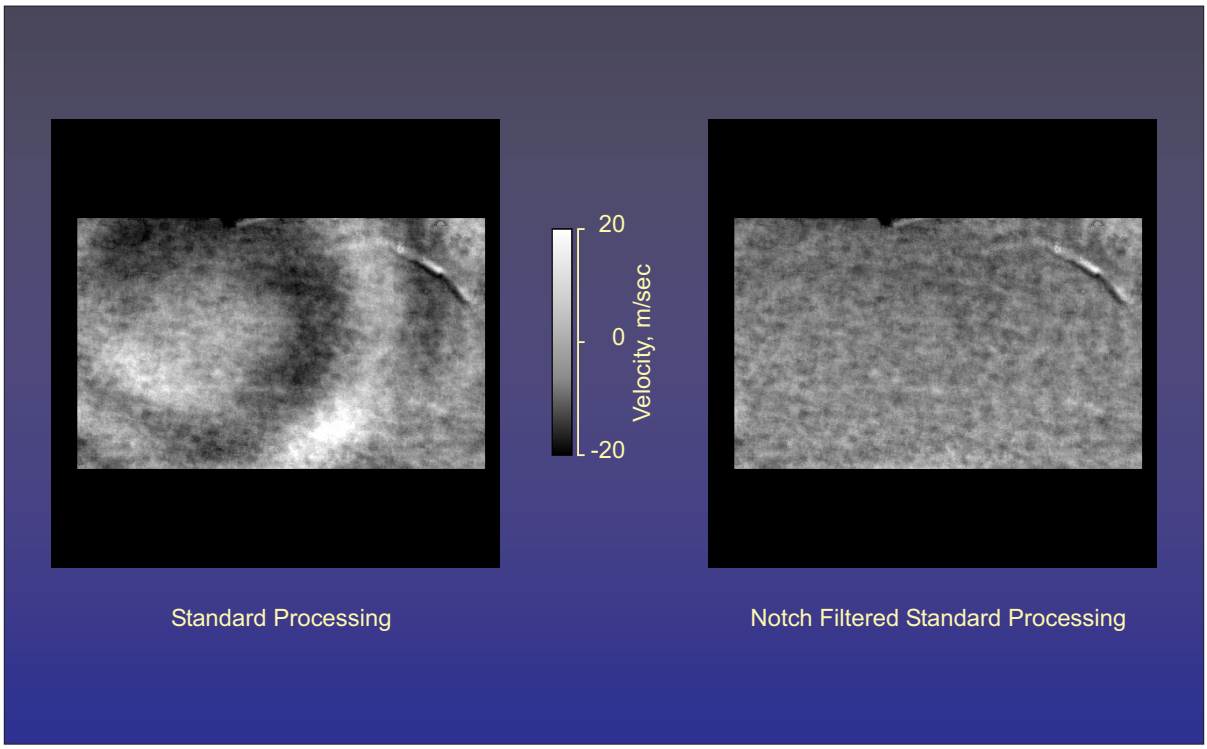

Figure 12. *U*-component velocity of the flow entering the tail rotor of a Comanche helicopter model before and after filtering the ring pattern.